Design and preliminary evaluation of a portable device for the measurement of bioimpedance spectroscopy

Yuxiang Yang[1], Jue Wang[1], Gang Yu[1], Feilong Niu[1] and Ping He[2]

[1] Key Laboratory of Biomedical Information Engineering of Education Ministry, School of Life Science and Technology, Xi'an Jiaotong University, Xi'an 710049, People's Republic of China
[2] Department of Biomedical, Industrial and Human Factors Engineering, Wright State University, Dayton, OH, USA

E-mail: yuxiangyang@mail.xjtu.edu.cn

Abstract

Portable bioimpedance spectroscopy (BIS) devices are of great value for monitoring the pathological status of biological tissues in clinical and home environments. The two traditional techniques for measuring complex bioimpedance, the bridge method and quadrature demodulation method, are either time-consuming or often associated with high cost, high power consumption, and large board space, and therefore are not ideally suitable for designing a portable device for BIS measurement. This paper describes a novel design of a portable BIS device based on the magnitude-ratio and phase-difference detection method and its implementation using the newest generation of analog electronic products which greatly decrease the complexity of both hardware and software. In order to improve the accuracy of the device, a three-reference calibration algorithm was applied. Experimental sweep-frequency measurements on RC circuits were carried out to preliminarily evaluate the performances of the device. The results obtained by the device were found to be in good agreement with the results measured by a commercial impedance analyzer HP4194, with an overall mean error of 0.014% in magnitude and $0.136°$ in phase over a frequency range of 20 kHz to 1 MHz.

Keywords: bioimpedance spectroscopy, magnitude-ratio and phase-difference detection method, gain-phase detector, three-reference calibration algorithm, sweep-frequency measurements

(Some figures in this article are in colour only in the electronic version)
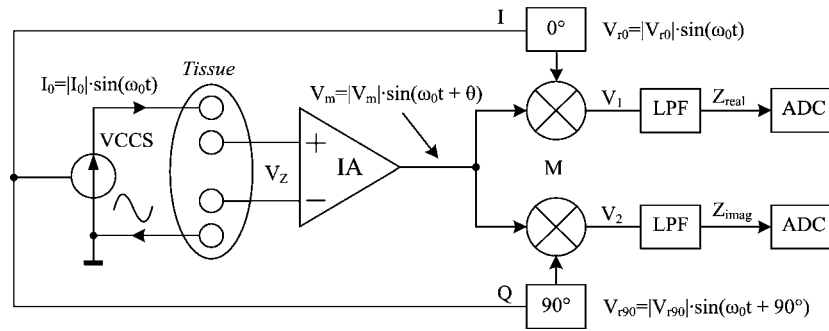
Figure 1. Block diagram of the conventional analog quadrature demodulation (AQD) method based on tetropolar structure. I_0—the excitation current source; V_{r0}—the in-phase (I) reference signal; V_{r90}—the quadrature (Q) reference signal; IA—instrumentation amplifier; M—multiplier (demodulator); LPF—low pass filter (used for removing sidebands at $2\omega_0$); Z_{real} and Z_{imag}—real part and imaginary components of complex impedance of tissue; ADC—A/D converter.

1. Introduction

Rapid and accurate measurement of the complex electrical impedance of bio-materials over a broad frequency range, a technique called bioimpedance spectroscopy (BIS), is of considerable importance for clinical diagnosis as well as for fundamental research, particularly in physiology and pathology. Analysis of the BIS can provide valuable information about the physiological status of living tissues such as ischemia (Kun *et al* 2003), lung edema (Mayer *et al* 2005), skin cancer (Åberg *et al* 2004) and intramuscular tumor (Skourou *et al* 2004). With the increasingly wide uses of the BIS technique, BIS measurement devices which are portable, compact, low cost, low power consumption, and capable of performing real-time measurement with adequate accuracy will be highly desirable both for hospital and home use.

There are basically two techniques for measuring the impedance of biologic tissue: the bridge method and quadrature demodulation (QD) method. The bridge method had traditionally been the most popular method with the major advantage of high measurement resolution and accuracy. However, this method is time-consuming due to the need for bridge balance and not well suited in situations where tissue impedance changes in time due to ongoing physiological processes (Steendijk *et al* 1993). Nowadays, QD or phase sensitive detector (PSD) methods are gaining popularity. The classical analog quadrature demodulation (AQD) technique, as shown in figure 1, is based on phase coherent demodulation and needs two channels of well-matched in-phase (I) and quadrature (Q) references. In AQD, the need for carefully avoiding any mismatch between the I and Q channels, which will cause large phase errors (Pallas-Areny and Webster 1993), may increase the complexity in circuit realization of AQD. With the aggressive development of DSP techniques, direct sampling of the signals at the carrier frequency has become possible in recent years, which enables the evolution of AQD to digital quadrature demodulation (DQD). DQD no longer requires the analog I and Q references. However, the need for high-speed ADCs and DSPs often leads to high costs and high power consumption because of the high sampling rate (Casanella *et al* 2005).

This paper describes a novel design of a portable BIS measurement system based on the magnitude-ratio and phase-difference detection (MRPDD) method, which provides a compact and cost-effective alternative for real-time impedance measurements. In the following sections, the principle of impedance measurement using the MRPDD method, and the implementation
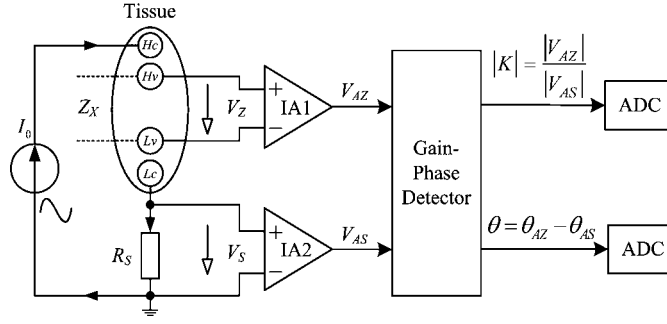
Figure 2. Impedance measurement principle based on the magnitude-ratio and phase-difference detection (MRPDD) method.

of the methods using the newest generation of analog electronic products, are first described in detail. A low cost, accurate three-reference calibration (TRC) algorithm based on quadratic Lagrange interpolation is then introduced which mathematically corrects the systematic errors. Experimental sweep-frequency measurements on RC circuits were carried out to evaluate the performances of the BIS device. Finally, the differences between the traditional QD method and the proposed MRPDD method based on the gain-phase detector (GPD) AD8302 are discussed.

2. Method

The principle of the proposed BIS device based on the MRPDD method is described in figure 2. In the figure, Z_X (hereafter, capital symbols represent complex quantities) represents the impedance of the tissue under measurement, and R_S is a reference resistor connected in series with Z_X. A sinusoidal excitation current I_0 flows through Z_X and R_S via a pair of current electrodes H_c and L_c. The voltage drop across Z_X (V_Z) is detected by a pair of voltage electrodes H_v and L_v and then amplified by instrumentation amplifier IA1, while the voltage drop across R_S (V_S) is amplified by another instrumentation amplifier IA2. Provided that the input impedances of IA1 and IA2 are infinite, there will be no current flowing through the two voltage electrodes, so the two output voltages of IA1 and IA2 can be expressed as:

$$\begin{cases} V_{AZ} = A_1 \cdot V_Z = A_1 \cdot I_0 \cdot Z_X \\ V_{AS} = A_2 \cdot V_S = A_2 \cdot I_0 \cdot R_S \end{cases} \tag{1}$$

where A_1 and A_2 are the gains of IA1 and IA2, respectively.

The gain-phase detector (GPD) compares V_{AZ} and V_{AS}, and outputs two dc voltages proportional to magnitude ratio $|K|$ and phase difference θ of the input voltages:

$$\begin{cases} |K| = \dfrac{|V_{AZ}|}{|V_{AS}|} \\ \theta = (\theta_{AZ} - \theta_{AS}). \end{cases} \tag{2}$$

From (1) and (2), the unknown impedance Z_X can be obtained:

$$Z_X = R_S \cdot \frac{V_Z}{V_S} = R_S \cdot \frac{A_2}{A_1} \cdot \frac{V_{AZ}}{V_{AS}} = R_S \cdot \frac{A_2}{A_1} \cdot |K| \angle \theta. \tag{3}$$
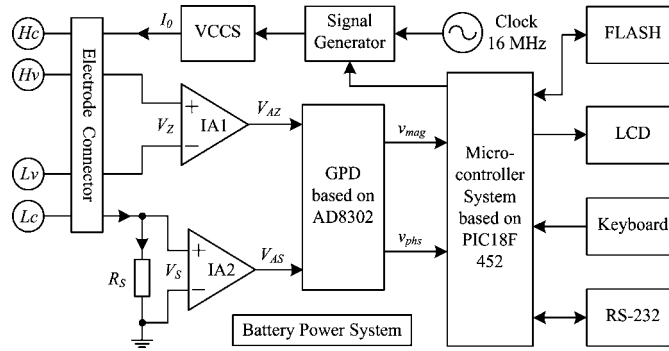
Figure 3. Structural diagram of the new-designed BIS device.

Figure 4. A photograph of the actual BIS device.

If the IA1, IA2 are constructed identically and have infinite input impedance, the gain ratio can be ideally assumed as $A_2/A_1 = 1$. Then (3) is simplified and the originally measured impedance Z_m is obtained as

$$Z_m = R_S \cdot |K| \angle \theta \tag{4}$$

where R_S is a standard resistor with known value, $|K|$ and θ are outputs of the GPD which can be sampled by ADCs and calculated by (8). Equations (1)–(4) are all based on the ideal hypothesis and disturbing factors are not considered. But in practice, the finite input impedance of IA1 and IA2, electrode contact impedance and stray capacitance will all contaminate the measurement precision. An equivalent measurement circuit model involving these disturbing factors will be analyzed and a three-reference calibration method will be introduced to correct the measurement errors in section 4.1.

3. System design

3.1. System overview

A portable BIS prototype device was designed and constructed based on the method described in section 2. Figure 3 provides a block diagram of the device and figure 4 shows an actual

Table 1. Summary of specifications of the BIS device.

Parameter	Range	Resolution
Frequency	20 kHz to 1 MHz	0.06 Hz
Impedance magnitude	9 Ω to 5.7 kΩ	0.36 Ω
Impedance phase	0° to −180°	0.049°
Mean magnitude error	0.014% (relative error)	
Mean phase error	0.136° (absolute error)	

picture of the device. The major building block of the BIS device as shown in figure 3 includes a signal (sine wave) generator, a voltage controlled current source (VCCS), two identical instrumentation amplifiers, a GPD and a microcontroller subsystem. The signal generator and the VCCS generate a sinusoidal current I_0 at pre-programmed frequencies in the range of 20 kHz to 1 MHz. The amplified voltage drops across the tissue and the reference resistor, denoted by V_{AZ} and V_{AS}, are fed into the GPD which outputs two dc voltages proportional to their magnitudes ratio and phase difference, respectively. The outputs of the GPD at each excitation frequency are sampled by the microcontroller system. The ultimate impedance magnitudes and phases can be calculated by software, displayed on LCD, stored in on-board memory or uploaded to a PC through a RS-232 interface. The BIS device is self-powered with a rechargeable battery. The weight of the entire system is about 0.5 kg and the overall size is close to that of a portable multimeter. Table 1 lists the operational specifications of the BIS device.

3.2. The circuit for generating the excitation source

The circuit for generating the excitation source includes a sine wave generator, a voltage controlled current source (VCCS) and a reference resistor R_S. The sine wave generator is based on AD9833 (Analog Devices, Norwood, MA), which is a low power programmable waveform generator based on the direct digital synthesis (DDS) technique, capable of producing a frequency- and phase-tunable sine signal referenced to a fixed-frequency precision clock source. The frequency of the output signal is determined by the number in a 28-bit frequency register FREQ using the following equation:

$$f_{OUT} = \frac{f_{CODE}}{2^{28}} f_{CLOCK} \tag{5}$$

where f_{CODE} is a number in FREQ and f_{CLOCK} is the frequency of the clock source (AD9833 data sheet 2003). In our BIS device, since the clock frequency is 16 MHz, a resolution of 0.06 Hz can be achieved. Data for FREQ are loaded through a 3-wire SPI interface from the microcontroller. With 10-lead MSOP package and only 25 mW power consumption, AD9833 is a good choice for portable electronic devices.

The output from the signal generator contains useful sine wave signals at the tuned frequency as well as undesirable alias signals. Hence, the output from the signal generator is connected to a low-pass, 'antialiasing' filter, whose frequency response should be 1 over the Nyquist band and 0 elsewhere. LTC1560-1 (Linear Technology Corporation, Milpitas, CA) which is an SO-8 package fully integrated continuous-time filter with a pin selectable cutoff frequency of 1 MHz or 500 kHz (LTC1560-1 data sheet 1997), is used as a low-pass filter following AD9833. In our BIS device, LTC1560-1 serves as a 5-pole elliptic filter with a cutoff frequency of 1 MHz.
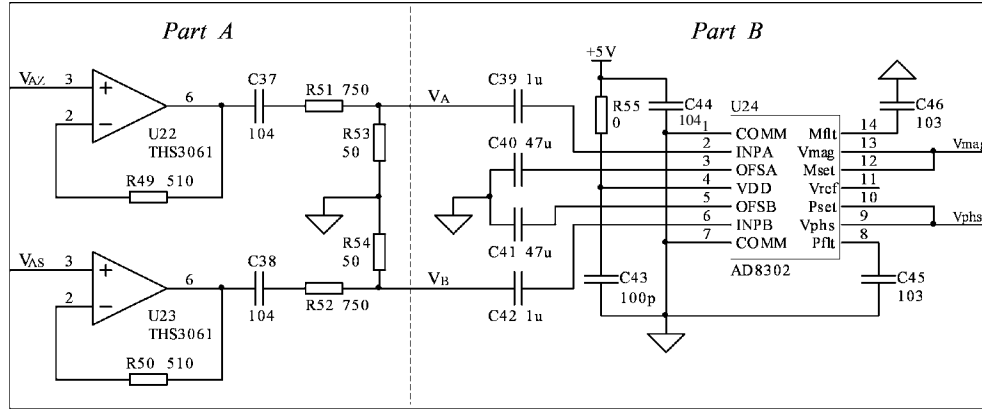
Figure 5. Practical circuit of the GPD based on AD8302.

The VCCS generates an output current proportional to the input voltage (output voltage of the sine wave generator). We designed a current source based on the AD844 (Analog Devices, Norwood, MA) current feedback amplifier according to the method proposed by Bragos *et al* (1994) with a peak value of 140 μA.

The reference resistor R_S, which is connected to electrode L_c in the excitation loop (figure 3), provides a reference voltage proportional to the current source I_0. R_S must be non-inductive and thus the voltage on it is in phase with I_0. A non-inductive resistor of 200 Ω was used in the BIS device.

3.3. Instrumentation amplifiers

IA1 and IA2 (in figure 3) are two identically constructed monolithic instrumentation amplifiers using INA163 (Texas Instruments, Dallas, TX), which has a high input impedance (6 M$\Omega \parallel$ 2 pF) and wide frequency bandwidth. The gain of IA1 and IA2 is set to 4 with the gain resistor $R_G = 2$ kΩ (INA163 data sheet 2000).

3.4. Gain-phase detector (GPD)

As the key component of the BIS device for precise complex impedance measurement, the GPD is based on AD8302 (Analog Devices, Norwood, MA), which is a fully integrated system for measuring either gain or loss over a ± 30 dB range scaled to 30 mV dB^{-1} and phase over $0°$ to $180°$ range scaled to 10 mV/degree. The ac-coupled input signals can range from -60 dBm (316 μV$_{peak}$) to 0 dBm (316 mV$_{peak}$) in a 50 Ω system, from low frequencies up to 2.7 GHz (AD8302 data sheet 2002). Figure 5 shows the actual connections circuit of the GPD based on the AD8302 used in our BIS device. The overall circuit consists of two parts, part A and part B.

3.4.1. Part A: input buffer. In order to match the 50 Ω input impedance of AD8302, input buffers are needed before the amplified signals V_{AZ} and V_{AS} (from instrumentation amplifier INA1 or INA2 in figure 3) entering the AD8302. In our device, two identical input buffers are constructed using two high speed, low output impedance amplifiers THS3061 (Texas Instruments, Dallas, TX), as shown in the left of figure 5. Each input buffer consists of a unity

gain buffer and a voltage attenuator with a 750 Ω resistor and a 50 Ω resistor. The attenuator matches the input impedance of AD8302 and reduces signal amplitude into the range between 316 μV_{peak} and 316 mV_{peak} for AD8302.

The input buffers, along with several other factors, determine the impedance measurement range. According to Faes's study (Faes *et al* 1999), the resistivity of most human tissues (except fat and bone) varies from about 150 to 675 Ω cm in the frequency range from 100 Hz to 10 MHz, while the whole-body impedance value changes from about 200 to 800 Ω (Lukaski and Siders 2003), and typically fall in the neighborhood of 500 Ω (Shiffman *et al* 1999). Hence, impedance devices with the available measurement range from several ohms to several kilo-ohms are adequate for both localized and whole-body measurements in most cases. For example, the commercial Quantum-II Desktop BIA system (RJL Systems Inc., Clinton Township, MI) has an impedance range of 0–1000 Ω both in resistance and reactance (RJL Systems website 2005). In our application, the measurement range of the BIS device is from about 9 Ω to 5.7 kΩ, which are estimated by the following equations:

$$\begin{cases} Z_{X\,\min} = \dfrac{316(\mu V)}{A \cdot G \cdot I_0(\mu A)}(\Omega) \\[2mm] Z_{X\,\max} = \min\left\{\dfrac{V_{O\,\max}(mV)}{G \cdot I_0(\mu A)}, \dfrac{316(mV)}{A \cdot G \cdot I_0(\mu A)}\right\}(k\Omega) \end{cases} \tag{6}$$

where A stands for the attenuator coefficient which can be calculated by R53/(R51 + R53), G is the gain of Z_X's amplifier IA1, I_0 is the excitation current amplitude and V_{Omax} is the output voltage amplitude of IA1. In figure 5, $A = 1/16$, $G = 4$ (see section 3.3), the current source $I_0 = 140\ \mu A$ (see section 3.2) and V_{Omax} (IA1 and IA2 in figure 3) is 3.2 V under ± 5 V power supply (INA163 data sheet 2000), which make $Z_{Xmin} \approx 9\ \Omega$ $Z_{Xmax} \approx 5.7$ kΩ. If a larger impedance range is needed, we can either decrease the values of A, G and I_0, or increase V_{Omax} by using a higher-voltage power supply for instrumentation amplifiers (as high as ± 15 V).

3.4.2. Part B: the AD8302. AD8302 comprises a phase detector and a closely matched pair of logarithmic amplifiers. It compares the two input signals V_A and V_B (in the middle of figure 5), and generates two output voltages: v_{mag} and v_{phs} which can be expressed as

$$\begin{cases} v_{mag} = \alpha_1 \cdot \log\left(\dfrac{|V_A|}{|V_B|}\right) + 900\,mV \\[2mm] v_{phs} = \alpha_2 \cdot (|\theta_A - \theta_B| - 90°) + 900\,mV \end{cases} \tag{7}$$

where α_1 and α_2 are two coefficients: $\alpha_1 = 600$ mV/decade (or 30 mV dB^{-1}), $\alpha_2 = -10$ mV/degree. Since the two input buffers and attenuators are constructed identically, the ratio of V_Z to V_S is equal to the ratio of V_{AZ} to V_{AS}. Hence the magnitudes ratio $|K|$ and phase differences θ in (2) can be solved from (7):

$$\begin{cases} |K| = \dfrac{|V_{AZ}|}{|V_{AS}|} = \dfrac{|V_A|}{|V_B|} = 10^{\frac{v_{mag} - 900\,mV}{600\,mV}} \\[2mm] \theta = \theta_A - \theta_B = \pm\left(\dfrac{900\,mV - v_{phs}}{10\,mV/degree} + 90°\right) \end{cases}. \tag{8}$$

Note that AD8302 does not distinguish between positive and negative phase differences (AD8302 data sheet 2002). But such an ambiguity does not cause the matter in our application because the tissue impedance is always capacitive. Hence, the phase formula in (8) can be

simplified as

$$\theta = -\left(\frac{900\,\text{mV} - v_{\text{phs}}}{10\,\text{mV/degree}} + 90°\right). \tag{9}$$

Therefore, according to (8) and (9), the complex impedance Z_{m} shown in (4) can be worked out in a polar-plane form by

$$\begin{cases} |Z_{\text{m}}| = R_{\text{S}} \cdot 10^{\frac{v_{\text{mag}} - 900\,\text{mV}}{600\,\text{mV}}} \\ \theta = -\left(\dfrac{900\,\text{mV} - v_{\text{phs}}}{10\,\text{mV/degree}} + 90°\right) \end{cases} \tag{10}$$

where $R_{\text{S}} = 200\,\Omega$ (section 3.2).

In figure 5, the two 47 μF capacitors C40 and C41, which are connected to the ac grounding pins OFSA and OFSB respectively, are the key components to set the high pass corner frequency of the internal offset compensation loop according to the formula f_{HP} (kHz) $= 2/C_{\text{C}}$ (μF), where C_{C} is the total capacitance from OFSA or OFSB to ground, including the internal 10 pF (AD8302 data sheet 2002). In this application, $C_{\text{C}} \approx 47$ μF, so $f_{\text{HP}} \approx 43$ Hz, which means that theoretically, AD8302 can work at frequency as low as 43 Hz (the feasible lower limit of frequency for the BIS device will be discussed in section 6). Output buffers with unity gain are necessary between the outputs of AD8302 (v_{phs} and v_{mag}) feeding into subsequent ADCs of the microcontroller system, aiming to provide enough current driving for the ADCs.

3.5. Microcontroller system

The microcontroller system is built around PIC18F452 (Microchip Technology Inc., Chandler, AZ) which performs many tasks with the on-board components, such as tuning DDS output frequencies, making A/D conversions using 12-bit ADC TLV2544 (Texas Instruments, Dallas, TX), calculating impedances and displaying outputs on 128 × 64 dot matrix LCD, inputting manipulator instructions through a keyboard (four press-buttons), saving results into FLASH memory AT45DB041 (Atmel Corporation, San Jose, CA) or uploading data to PC via RS-232 serial port.

The 12 bit ADC can achieve a 0.49 mV resolution referencing to an internal reference voltage of 2.0 V in TLV2544. This means that the BIS device can achieve a resolution of 0.016 dB (or 0.18% relative change) in gain or of 0.36 Ω in tested impedance magnitude (0.18% of the 200 Ω R_{S}) (base on the scale of 30 mV dB^{-1}), and a resolution of 0.049° in phase measurement (based on the scale of 10 mV/degree).

AT45DB041 is a serial interface Flash memory with 2048 pages, 264 bytes per page, enough to store samples of as many as 2000 sweep-frequency measurements, each measurement generating 32 samples at 32 frequency points from 20 kHz to 1 MHz.

3.6. Software design

The software of the BIS device was written in C language and developed in MPLAB (version 7.22, Microchip Technology Inc., Chandler, AZ) integrated development environment along with PICC C-18 compiler (HI-TECH Software, Gilroy, CA). The hardware emulator is MPLAB ICD2. The program provides a friendly human-machine interface which can generate a graphic display on the LCD of the impedance magnitude spectrum, impedance phase spectrum or Cole-Cole plot.
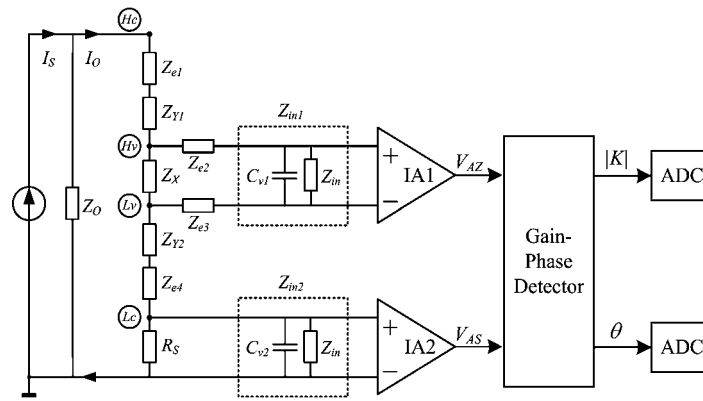
Figure 6. Equivalent circuit model of the four-terminal measurement for the proposed BIS device based on the MRPDD method. I_S—current source; I_0—output the current source; C_{v1}, C_{v2}—stray capacitances; Z_O—output impedance of the current source; Z_{e1} to Z_{e4}—electrode impedances; Z_{Y1}, Z_{Y2}—indifferent impedances between current and voltage electrodes; Z_X—measured impedance; Z_{in}—internal differential input impedance of the instrumentation amplifiers IA1 and IA2; Z_{in1}, Z_{in2}—overall input impedance of IA1 and IA2; H_c, H_v, L_v and L_c—the four electrodes.

4. System calibration

4.1. Calibration theory

System calibration plays an important role in achieving accurate measurements since measurement errors are nearly inevitable. Random errors in measurements can be eliminated by averaging and smoothing procedure, but systematic errors often cause a consistent bias that cannot be removed by averaging (Liu *et al* 1999). In the BIS device, the systematic errors mainly come from the analog input/output channels, such as electrodes, cables and amplifiers. Figure 6 shows an equivalent circuit model of the analog channels for the proposed BIS system.

In figure 6, cable capacitances are neglected because of the use of screen driving separately for each of the four cables in the BIS device. In principle, the driven shield is held at the same signal level as the signal line itself by means of a buffer amplifier, which can reject the capacitive current even when the cable capacitance still exists (Riu *et al* 1996, Li *et al* 1996). However, stray capacitances, which often derive between parallel signal leads, will seriously reduce the measurement accuracy, especially at high frequencies (Riu *et al* 1996). In figure 6, C_{v1} represents stray capacitance simulating crosstalk between the two voltage cables and stray around IA1 on board, while C_{v2} stands for stray capacitance around IA2 on board. The crosstalk stray capacitances between neighboring current and voltage cables, not shown in the figure, are less important and can be neglected as long as the impedances between the current and voltage electrodes are low (Scharfetter *et al* 1998). The power line interference (50 or 60 Hz), as a major source of errors in biopotential measurements (Spinelli *et al* 2006), is avoided by the use of battery power in the BIS device.

The model shown in figure 6 may be too simple to simulate the real behavior of the device, but it provides us with an approach to qualitatively analyze the measurement errors.

Let $Z_{ev} = Z_{e2} + Z_{e3}$, V_{AZ} and V_{AS} shown in figure 6 can be expressed as

$$
\begin{cases}
V_{AZ} = A_1 \cdot I_0 \cdot \dfrac{Z_X \cdot Z_{in1}}{Z_X + Z_{ev} + Z_{in1}} \\[2mm]
V_{AS} = A_2 \cdot I_0 \cdot \dfrac{R_S \cdot Z_{in2}}{R_S + Z_{in2}}
\end{cases}
\tag{11}
$$

where Z_{in1} and Z_{in2} are the overall input impedances of IA1 and IA2, including their internal differential input impedance Z_{in} paralleled with their stray capacitances C_{v1} and C_{v2}, respectively. Z_{in} can also be modeled as a very large resistor paralleled with a little input capacitance, which is 6 MΩ ‖ 2 pF for the INA163 in the BIS device. Similar to (3), the true value of the measured impedance, Z_X, can be eventually obtained:

$$
Z_X = Z_m \cdot \frac{A_2}{A_1} \cdot \frac{Z_{in2} \cdot (Z_X + Z_{ev} + Z_{in1})}{Z_{in1} \cdot (R_S + Z_{in2})}
\tag{12}
$$

where Z_m is the apparently measured impedance expressed by (4).

In (12), the relationship between the true value Z_X and the apparent value Z_m of the measured impedance is determined by amplifier input impedances Z_{in1} and Z_{in2}, amplifier gains A_1 and A_2, voltage electrode impedance Z_{ev}, reference resistor R_S and the measured impedance Z_X itself. At low frequencies, Z_{in1} and $Z_{in2} \gg Z_{ev}$, R_S and Z_X, we can assume that there is a linear relationship between Z_X and Z_m. With the increasing of frequency, Z_{in1} and Z_{in2} will be decreased dramatically due to stray capacitance and the input capacitances of IA1 and IA2. Under this circumstance, the above assumptions will be no longer applicable, and the relationship between Z_X and Z_m becomes a complicated complex nonlinear function variable with frequencies. Moreover, the values of the different parameters in (12) are not known exactly and variable with frequency, which means that the functions between Z_X and Z_m may be much different at different frequencies.

The aim of calibration is to find out the mapping relation between Z_X and Z_m at each interested frequency point. Practically, calibration is performed by measuring one or several references using the measurement device. With the measured values Z_m and their standard values Z_X of the reference(s), an approximative function can be established to fit the relation between Z_X and Z_m. Calibration with one known resistor or RC network has commonly been used in commercial bioimpedance instruments, such as XITRON 4000B (Xitron Technologies Inc., San Diego, CA) (Scharfettery *et al* 1998) and RJL 101A (RJL Systems Inc., Clinton Township, MI) (Lukaski and Siders 2003). However, this single reference calibration was proved insufficient and poor accuracy was found at frequencies above 500 kHz (Scharfettery *et al* 1998). Obviously, nonlinear relationship occurs at high frequencies and cannot be corrected by a single reference calibration method.

In our application, a three-reference calibration (TRC) algorithm proposed by Liu (1999) was adopted. This algorithm is based on an assumption that there is a quadratic relation between the measured value Z_m and the true value Z_X: $Z_X = k_2 Z_m^2 + k_1 Z_m + k_0$. With the use of three calibration references (RC circuits), their true values (Z_{r0}, Z_{r1}, Z_{r2}) and original measured values (Z_{mr0}, Z_{mr1}, Z_{mr2}) by the BIS device can be obtained, which fixes three points on the quadratic curve with known coordinate values (Z_{mr0}, Z_{r0}), (Z_{mr1}, Z_{r1}) and (Z_{mr2}, Z_{r2}). These three known points can then uniquely determine the relation between Z_X and Z_m by a quadratic Lagrange interpolation (Liu *et al* 1999):

$$
\begin{aligned}
Z_X = {} & Z_{r0} \frac{(Z_m - Z_{mr1})(Z_m - Z_{mr2})}{(Z_{mr0} - Z_{mr1})(Z_{mr0} - Z_{mr2})} + Z_{r1} \frac{(Z_m - Z_{mr2})(Z_m - Z_{mr0})}{(Z_{mr1} - Z_{mr2})(Z_{mr1} - Z_{mr0})} \\
& + Z_{r2} \frac{(Z_m - Z_{mr0})(Z_m - Z_{mr1})}{(Z_{mr2} - Z_{mr0})(Z_{mr2} - Z_{mr1})}.
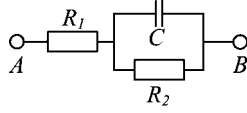\end{aligned}
\tag{13}
$$

Figure 7. Two-terminal topology of the RC circuits.

Table 2. Parameters of the three calibration reference circuits.

	R_1 (Ω)	R_2 (Ω)	C (nF)	f_C (kHz)	θ_{peak} ($°$)
Z_{r0}	82	27	68	100	-8.13
Z_{r1}	180	243	10	100	-23.76
Z_{r2}	324	953	3.3	100	-36.53

Before calibration, the three reference standard values (Z_{r0}, Z_{r1}, Z_{r2}) at each interested frequency point can be obtained by a precise impedance analyzer (section 4.2), while their measured values ($Z_{mr0}, Z_{mr1}, Z_{mr2}$) at the same frequencies can be collected through calibration measurements using the BIS device (section 4.3). Therefore, at each frequency point, a function between Z_X and Z_m can be established in (13) separately with their relevant six constants (Z_{r0}, Z_{r1}, Z_{r2}) and ($Z_{mr0}, Z_{mr1}, Z_{mr2}$). Finally, the apparently measured impedance Z_m calculated from (4) can be corrected to Z_X through (13). Note that values of all symbols in (13) are in complex form.

4.2. RC calibration circuits

We use three RC circuits having the reference impedances Z_{r0}, Z_{r1} and Z_{r2} for calibration. Each RC circuit consists of two resistors and a capacitor, as shown in figure 7, with the hypothesis that the extra-cellular liquid and intra-cellular liquid act like resistors and the cell membrane like an capacitor in biological tissues (Neves and Souza 2000). The RC circuit has a characteristic frequency f_C where phase θ reaches its peak θ_{peak}. The f_C and θ_{peak} can be evaluated by

$$\begin{cases} f_C = \dfrac{1}{2\pi C}\sqrt{\dfrac{R_1 + R_2}{R_1 R_2^2}} \\[2ex] \theta_{\text{peak}} = -\arctan\left(\dfrac{1}{2}\sqrt{\dfrac{R_2^2}{R_1(R_1 + R_2)}}\right) \end{cases}. \tag{14}$$

Table 2 lists the nominal values of R_1, R_2 and C for the Z_{r0}, Z_{r1} and Z_{r2}, which are carefully chosen to give the same characteristic frequency f_C at 100 kHz. In each RC circuit, R_1 and R_2 are 1/4 Watt metal-film resistors with $\pm 1\%$ tolerance, and C is a low-loss metalized polyester film capacitor with $\pm 5\%$ tolerance.

Three practical RC circuits were measured one by one on an impedance analyzer HP4194A (Hewlett-Packard, Palo Alto, CA), whose outputs were used as the constants Z_{r0}, Z_{r1} and Z_{r2} in (13). The device used to connect the reference circuits with HP4194A is Hewlett-Packard Model 16047C test fixture. The measured impedance spectra data at 32 frequency points, which space throughout a 20 kHz to 1 MHz range: 20, 25, 30, 35, 40, 45, 50, 55, 60, 65, 70, 75, 80, 85, 90, 95, 100, 150, 200, 250, 300, 350, 400, 450, 500, 550, 600, 650, 700,
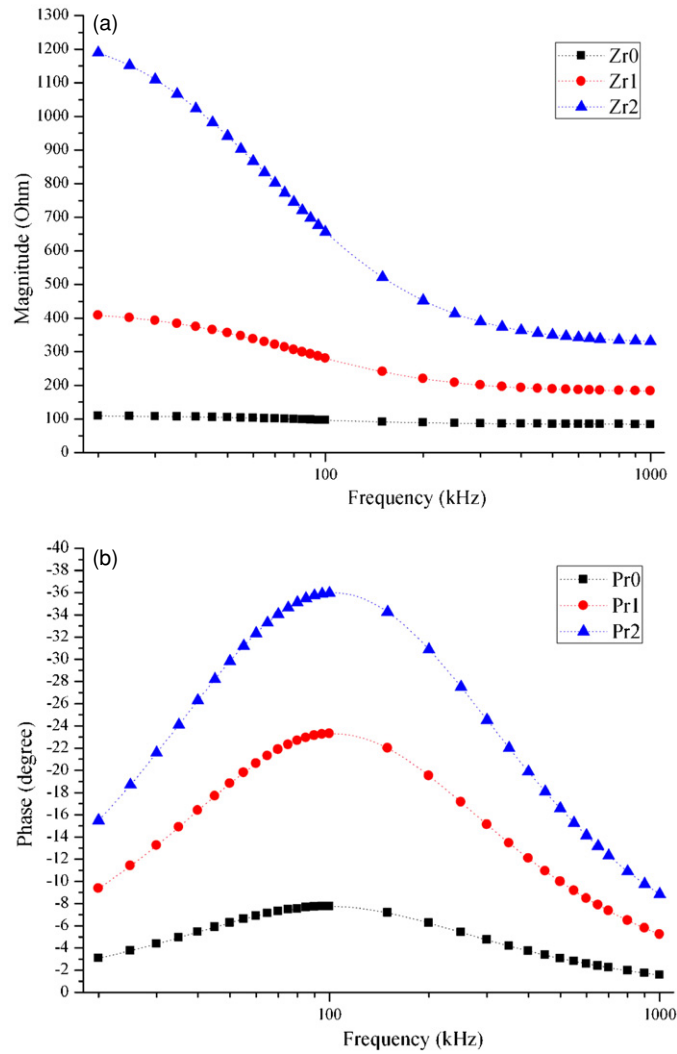
Figure 8. The standard magnitude-frequency and phase-frequency characteristics of the three RC calibration references at 32 selected frequency points measured by HP4194: (a) the magnitude-frequency characteristics curve, (b) the phase-frequency characteristics curve.

800, 900, 1000 kHz, were recorded and stored into the on-board FLASH memory. The magnitude-frequency and phase-frequency characteristics were plotted in figures 8(a) and (b), respectively.

4.3. Calibration measurements

Calibration measurements must be performed by the BIS device, whose measurement results on the three reference circuits will act as the constants Z_{mr0}, Z_{mr1} and Z_{mr2} in (13). Circuits to be measured on the BIS device must be first changed into the form of the four-terminal configuration as shown in figure 9 by adding two 51 Ω resistors to each of the origin reference

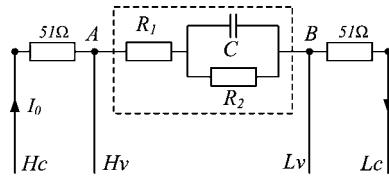**Figure 9.** Four-terminal topology of the RC circuit measurements. The two 51 Ω resistors are used to simulate the resistance between the current output and voltage measurement terminals.

Table 3. Parameters of the three measurand circuits.

	R_1 (Ω)	R_2 (Ω)	C (nF)	f_C (kHz)	θ_{peak} (°)
Z_{x0}	200	200	22	51	-19.5
Z_{x1}	240	220	10	100	-18.2
Z_{x2}	150	150	10	150	-19.5

circuits. The two 51 Ω resistors are used to simulate the resistance between the current output and voltage measurement electrodes (Bao *et al* 1993), while the part between A and B (framed by dashed in figure 9) is one of the RC calibration references just as shown in figure 7. The four-terminal RC circuit is connected to the BIS device through four driven shielded cables with four clamps.

Three sweep-frequency measurements on the calibration circuits were performed using the BIS device. Each sweep-frequency measurement collects impedance data at all of the same 32 frequency points as those chosen in figure 8. The result at each frequency point is averaged by sampling 128 periods, which makes the random errors negligible. The complex results of calibration measurements, Z_{mr0}, Z_{mr1} and Z_{mr2}, which were calculated according to (10) with the sampled values of v_{phs} and v_{mag}, were stored as constants in the on-board FLASH memory. When computing the calibrated value of Z_X at the same frequency point according to (13) for the originally measured value Z_m, both the stored calibration measurement values Z_{mr0}, Z_{mr1}, Z_{mr2} and the standard values Z_{r0}, Z_{r1}, Z_{r2} (which were previously measured and stored as described in section 4.2) at a certain frequency point will be read out.

5. Preliminary evaluation

In order to evaluate the performance of the BIS device, we prepared three other RC circuits Z_{x0}, Z_{x1} and Z_{x2} as measurands, whose circuit topology is the same as shown in figure 7, and whose nominal values of R_1, R_2 and C parameters are listed in table 3. The three RC circuits have different characteristic frequencies at 51 kHz, 100 kHz and 150 kHz, which typically locate in the characteristic frequency range spanned by different types of biological tissues (Osypka and Gersing 1995).

The three RC circuits with the two-terminal topology (figure 7) were first tested on the HP4194, and the results at the same 32 frequency points as used in the calibration procedure were regarded as their standard values: Z_{x0}, Z_{x1} and Z_{x2}. Two 51 Ω resistors were then added to each circuit to establish a four-terminal configuration as shown in figure 9. Three sweep-frequency measurements using the BIS device on the three four-terminal RC circuits were performed and the results at the same 32 frequency points were recorded as Z_{mx0}, Z_{mx1} and Z_{mx2}. Finally, calibration computations were carried out at each frequency point, and
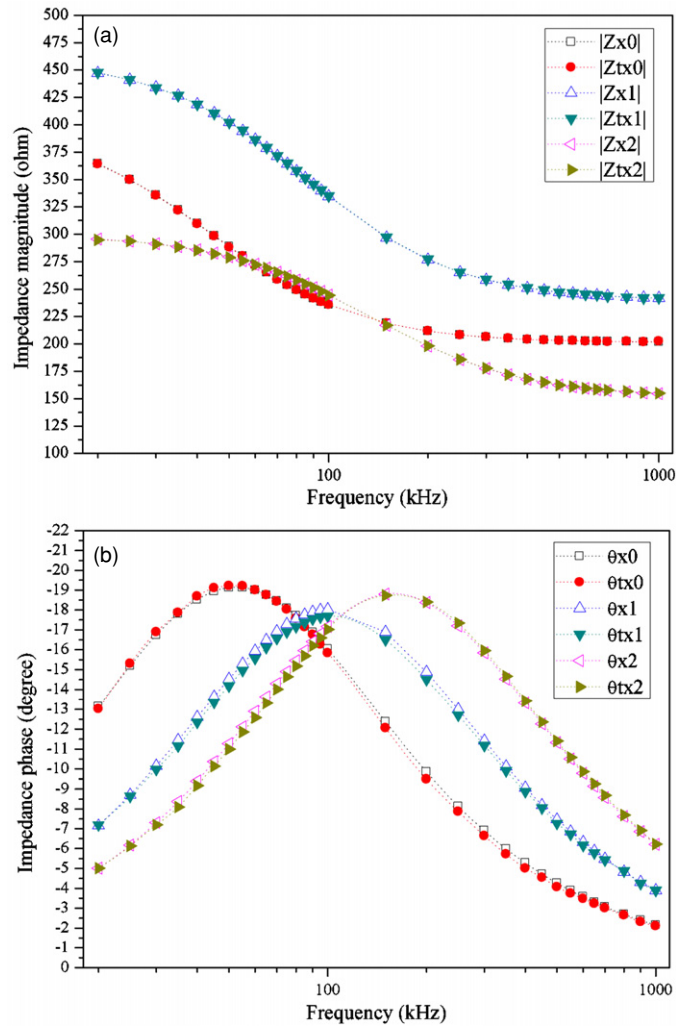
Figure 10. The measurement results on three RC circuits: (a) the standard impedance magnitudes measured by HP4194 and the values measured by the BIS device, (b) the standard and the measured phases, (c) the relative errors of impedance magnitudes, (d) the absolute errors of phases.

the calibrated values Z_{tx0}, Z_{tx1} and Z_{tx2} were obtained. At each frequency, three calibration computations were independently performed according to (13), using their corresponding originally measured values Z_{mx0}, Z_{mx1} and Z_{mx2}, respectively. For example, when computing the Z_{tx0}, the Z_m in (13) was substituted by the uncorrected value of Z_{mx0}, and the corresponding corrected value Z_{tx0} was obtained.

The performances of the BIS device were evaluated by comparing the deviations of the calibrated values Z_{tx0}, Z_{tx1} and Z_{tx2} referenced to the standard values of Z_{x0}, Z_{x1} and Z_{x2}. The results were shown in figure 10, in which figure 10(a) depicts both the standard impedance magnitude values Z_{xi} and the calibrated values Z_{txi}, figure 10(c) shows the relative errors of the impedance magnitudes calculated by $((|Z_{txi}| - |Z_{xi}|)/|Z_{xi}|) \times 100\%$, figure 10(b) shows the standard impedance phases θ_{xi} and the measured phases θ_{txi}, and figure 10(d) shows the absolute errors of the phases calculated by $(\theta_{txi} - \theta_{xi})$, $(i = 0, 1, 2)$.
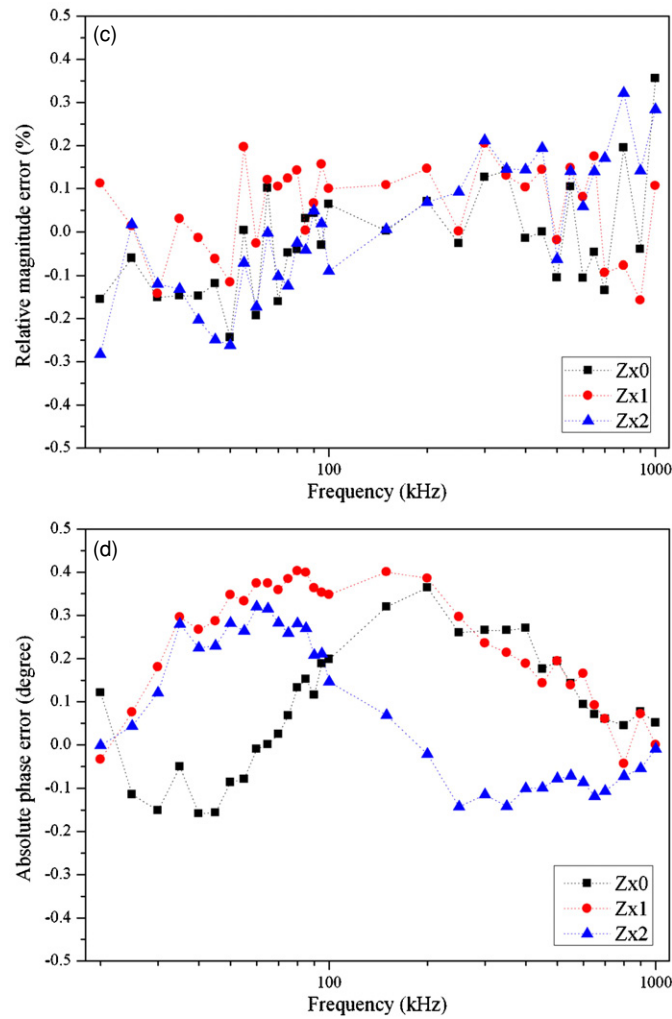
Figure 10. (Continued.)

In figure 10(c) the overall mean magnitude error is 0.014% with a maximum error of 0.36%, while in figure 10(d) the overall mean phase error is 0.136° with a maximum error of 0.4° over the 32 frequency across the three measurands. The maximum absolute error of magnitude is 0.84 Ω, while the maximum relative error of phase reaches 5.13%.

6. Discussion

The performance of the newly-designed BIS device, which is based on the MRPDD method and essentially incorporates an analog demodulation scheme like the AQD method (figure 1), relies basically on the capability of the GPD. The main difference between the MRPDD and AQD methods lies in the fact that the MRPDD method focuses on detecting relative amplitude (i.e. gain or ratio) and phase, while the AQD method aims to measure the real and imaginary parts of the impedance-coupled signals. Previous techniques for measuring
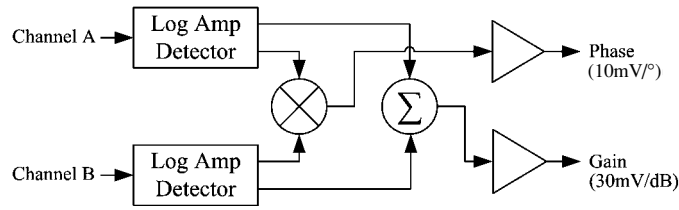
Figure 11. The schematic block diagram of the GPD chip AD8302.

gain and phase required complex and expensive instruments or circuitry. Fortunately, now this task can be easily achieved through a compact integrated circuit (IC) AD8302 which is used as the GPD in our application. The AD8302 is claimed to be the industry's first monolithic IC designed to accurately measure both gain and phase difference between two independent signals. Figure 11 shows the schematic block diagram of the AD8302 chip, which comprises a pair of accurately matched demodulating logarithmic amplifiers and a novel multiplier-style phase detector (Cowles and Gilbert 2001). Since both logarithmic amplifiers are fabricated on the same die with symmetric structure, errors associated with each stage track each other and thereby can be effectively counteracted. Thereby, mismatches owing to multi-chip discrete solutions in the traditional AQD method, which may significantly reduce measurement accuracy, could be inherently avoided in the MRPDD method based on the monolithic AD8302. This advantage may become more significant when constructing AD8302-based BIS devices with upper frequency limits higher than 1 MHz in the future.

The BIS device, however, does have two disadvantages due to the shortcomings of the AD8302 itself. Firstly, positive and negative phases cannot be distinguished, as mentioned in section 3.4.2. Additional circuitry to check the direction of phase will be needed if phases with both directions are to be detected. Secondly, it is found in experiments that the BIS device cannot perform measurements under frequencies below 20 kHz with acceptable accuracy, whereas bioimpedance spectra below 20 kHz contain useful information (Osypka and Gersing 1995). This phenomenon was observed by a digital oscilloscope Tektronix TDS2014 (Tektronix, Inc., OR, USA). When the input signals were below 20 kHz, the AD8302's outputs of both the gain and phase had large deviations from the true values calculated according to the actual input waveforms on the screen of the oscilloscope. In this case, the calibration procedure (section 4) becomes helpless since the fundamental component of the BIS device, the AD8302, cannot work well. Obviously, the AD8302 which was initiated for radio frequency (RF) and intermediate frequency (IF) applications may lack adequate technical consideration for audio-frequency uses, though the AD8302's high pass corner frequency f_{HP} is set to as low as 43 Hz theoretically (see section 3.4.2). New quasi-AD8302 chips with better performance in low-frequency range are expected to broaden the lower frequency range for the BIS device.

Traditionally, the performance of VCCS plays an important role for precise bioimpedance measurements where infinite output impedance is expected so that the load current I_0 remains a constant for different impedance loads, and many attempts were made to obtain the highest possible output impedance (Bragos *et al* 1994, Denyer *et al* 1994, Ross *et al* 2003). In our BIS device, however, the requirement for the performance of the VCCS may be degraded. As shown in figure 6, the reference resistor R_S, which is connected in serial with the sample Z_X, tracks changes of current source I_0 both in magnitude and phase in time and provides a dynamic referencing base for the gain-phase detector AD8302. The output current I_0 will be decreased when its output impedance Z_O becomes smaller. But this will hardly influence the measured results since the voltages on Z_X and R_S will simultaneously move with I_0 and the ratio between

them, namely the magnitude ratio $|K|$ and phase difference θ in (4), is unchanged. Hence, it is reasonable to affirm that the fluctuation of I_0 will not influence the measurement accuracy as long as I_0 locates in the effective range in which the electric property of the samples does not change.

7. Conclusion

To conclude our study we would like to underline that the preliminary experimental results confirm the applicability of the proposed BIS device based on MRPDD method. The MRPDD method presented in this paper is very simple and easy to implement with the use of monolithic GPD AD8302, and the low-cost TRC algorithm is effective. Such a simple design based on the newest generation of highly integrated electronic components provides a wide frequency range, small circuitry dimensions, small power consumption and low cost with a comparable accuracy. This new BIS device provides a feasible advantage over the traditional bioimpedance measurement systems, based on either AQD or DQD methods, by simplifying the electronics and reducing the systems cost.

References

Åberg P, Nicander I, Hansson J, Geladi P, Holmgren U and Ollmar S 2004 Skin cancer identification using multifrequency electrical impedance—a potential screening tool *IEEE Trans. Biomed. Eng.* **51** 2097–102
AD8302 Data Sheet 2002 Analog Devices, Corporate Headquarters, One Technology Way, PO Box 9106, Norwood, MA 02062-9106, USA (available in PDF format from http://www.analog.com/UploadedFiles/Data_Sheets/797075782AD8302_a.pdf)
AD9833 Data Sheet 2003 Analog Devices, Corporate Headquarters, One Technology Way, PO Box 9106, Norwood, MA 02062-9106, USA (available in PDF format from http://www.analog.com/UploadedFiles/Data_Sheets/37150134474160AD9833_a.pdf)
Bao J-Z, Davis C C and Schmukler R E 1993 Impedance system spectroscopy of human erythrocytes calibration and nonlinear modeling *IEEE Trans. Biomed. Eng.* **40** 364–78
Bragos R, Rosell J and Riu P 1994 A wide-band AC-coupled current source for electrical impedance tomography *Physiol. Meas.* **15** A91–A99
Casanella R, Casas O and Pallàs-Areny R 2005 Differential synchronous emodulator for modulating sensors and impedance measurements *Meas. Sci. Technol.* **16** 1637–43
Cowles J and Gilbert B 2001 Accurate gain/phase measurement at radio frequencies up to 2.5 GHz *Analog Dialogue* **35** (October) (available in PDF format from http://www.analog.com/library/analogDialogue/archives/35-05/AD8302/AD8302.pdf)
Denyer C W, Lidgey F J, Zhu Q S and McLeod C N 1994 A high output impedance current source *Physiol. Meas.* **15** A79
Faes T J C, Meij H A v d, Munck J C d and Heethaar R M 1999 The electric resistivity of human tissues (100 Hz-10 MHz): a meta-analysis of review studies *Physiol. Meas.* **20** R1–R10

INA163 Data Sheet 2000 Texas Instruments, Company Headquarters, 12500 TI Boulevard, PO Box 660199, Dallas, TX 75243-4136, USA (available in PDF format from http://www-s.ti.com/sc/ds/ina163.pdf)

Kun S, Ristic B, Peura R A and Dunn R M 2003 Algorithm for tissue ischemia estimation based on electrical impedance spectroscopy *IEEE Trans. Biomed. Eng.* **50** 1352–9

Li J H, Joppek C and Faust U 1996 Fast EIT data acquisition system with active electrodes and its application to cardiac imaging *Physiol. Meas.* **17** A25–A32

Liu J-G, Frühauf U and Schönecker A 1999 Accuracy improvement of impedance measurements by using the self-calibration *Measurement* **25** 213–25

LTC1560–1 Data Sheet Linear Technology, Corporate Headquarters 1630 McCarthy Blvd. Milpitas, CA 95035-7417, USA (available in PDF format from http://www.linear.com/pc/downloadDocument.do?navId= H0,C1,C1154,C1008,C1148,P1547,D3990)

Lukaski H C and Siders W A 2003 Validity and accuracy of regional bioelectrical impedance devices to determine whole-body fatness *Nutrition* **19** 851–7

Mayer M, Brunner P, Merwa R and Scharfetter H 2005 Monitoring of lung edema using focused impedance spectroscopy: a feasibility study *Physiol. Meas.* **26** 185–92

Neves C E B and Souza M N 2000 A method for bio-electrical impedance analysis based on a step-voltage response *Physiol. Meas.* **21** 395–408

Osypka M and Gersing E 1995 Tissue impedance spectra and the appropriate frequencies for EIT *Physiol. Meas.* **16** A49–A55

Pallas-Areny R and Webster J G 1993 Bioelectric impedance measurements using synchronous sampling *IEEE Trans. Biomed. Eng.* **40** 824–9

Riu P J, Bragós R and Rosell J 1996 Broadband quasi-differential multifrequency electrical impedance imaging system *Physiol. Meas.* **17** A39

RJL Systems Inc. 2005 website http://www.rjlsystems.com/products/more_desktop.shtml

Ross A S, Saulnier G J, Newell J C and Isaacson D 2003 Current source design for electrical impedance tomography *Physiol. Meas.* **24** 509–16

Scharfettery H, Hartingery P, Hinghofer-Szalkayz H and Hutteny H 1998 A model of artefacts produced by stray capacitance during whole body or segmental bioimpedance spectroscopy *Physiol. Meas.* **19** 247–61

Shiffman C A, Aaron R, Amoss V, Therrien J and Coomler K 1999 Resistivity and phase in localized BIA *Phys. Med. Biol.* **44** 2409–29

Skourou C, Hoopes P J, Strawbridge R R and Paulsen K D 2004 Feasibility studies of electrical impedance spectroscopy for early tumor detection in rats *Physiol. Meas.* **25** 335–46

Spinelli E M, Mayosky M A and Pallás-Areny R 2006 A practical approach to electrode-skin impedance unbalance measurement *IEEE Trans. Biomed. Eng.* **53** 1451–3

Steendijk P, Mur G, Velde E T V D and Baan J 1993 The four-electrode resistivity technique in anisotropic media: theoretical analysis and application on myocardial tissue in vivo *IEEE Trans. Biomed. Eng.* **40** 1138–48